REVIEW / SYNTHÈSE

The flexible atomic code

Ming Feng Gu

Abstract: We describe a complete software package for the computation of various atomic data such as energy levels; radiative transition; collisional excitation; ionization by electron impact, photoionization, autoionization; and their inverse processes radiative recombination and dielectronic capture. The atomic theoretical background and numerical techniques associated with each process are discussed in detail. Sample applications and results are presented.

PACS Nos.: 31.15.−p, 32.70.Cs, 34.80.Kw, 32.80.Fb, 32.80.Dz

Résumé : Nous décrivons un ensemble complet de programmes informatiques pour calculer diverses quantités atomiques, comme les niveaux d'énergie, les transitions radiatives, l'excitation et l'ionisation par collision électronique, la photoionisation, l'autoionisation et leurs mécanismes radiatifs inverses de recombinaison et de capture diélectronique. Nous repassons en détail les bases théoriques et les techniques informatiques associées à chaque processus atomique. Nous présentons des exemples d'utilisation avec leurs résultats.

[Traduit par la Rédaction]

1. Introduction

In this paper, we review the flexible atomic code (FAC). FAC is a complete software package for the computation of various atomic radiative and collisional processes. Since its introduction, the package has been used successfully for modeling the spectral emission from astrophysical plasmas. For example, ref. 1 investigates indirect level population processes of iron L-shell ions in optically thin plasmas, such as those present in stellar coronae and clusters of galaxies; refs. 2–4 use FAC to calculate radiative and dielectronic recombination rates for a number of astrophysically important ions and the X-ray line radiation following such recombination processes in low temperature, photoionized plasmas, which are often present in active galactic nuclei (AGN), and X-ray binaries (XRB). FAC has also been used to model the emission from magnetic fusion plasmas [5]. Laboratory astrophysics experiments performed at the Livermore electron beam ion traps (EBITs) have tested multiple aspects of the package, and excellent agreement between FAC results and laboratory data were found [6–8]. Hansen [9] used FAC results to analyze the X-ray spectra of krypton clusters irradiated by high-intensity femtosecond laser pulses. Zhong et al. [10] used FAC data to investigate the driver-pulse configuration of the Ni-like Ta X-ray laser. The software package has also been adopted by numerous researchers around the world. Uses include the calculations of magnetic sublevel populations for the development of plasma polarization diagnostics [11] and the determination of density-dependent line ratios [12, 13]. FAC data have also been included in databases such as CHIANTI [14].

FAC employs a fully relativistic approach based on the Dirac equation, which allows its application to ions with large values of nuclear charge. Currently, FAC is able to treat radiative transition, direct collisional excitation, and ionization by electron impact nonresonant photoionization and radiative recombination, autoionization and dielectronic recombination. These processes are essential for the interpretation of laboratory and astrophysical spectroscopic data. The main goal of creating such a comprehensive package is to integrate various atomic processes within a single theoretical framework, ensure the self-consistency between different parts, and provide a uniform flexible and easy-to-use user interface for accessing all computational tasks.

Many computer programs now exist for the calculation of atomic processes, using either nonrelativistic approximations (some including relativistic effects through the Breit–Pauli Hamiltonian) or fully relativistic methods. Most of them are concerned mainly with atomic structure and bound–bound processes, for example, the nonrelativistic configuration interaction codes CIV3 [15] and SUPERSTRUCTURE [16], the widely used program of Cowan [17], the multiconfiguration Hartree–Fock (MCHF) program of Fisher et al. [18], and the multiconfiguration Dirac–Fock (MCDF) code of Grant et al. [19]. Many newer programs for continuum processes make use of the output from these structure codes for bound-state wave functions. This sometimes leads to a different treatment of continuum states from that of bound states. More importantly, the communication between different programs tends to complicate the user interface, and makes it difficult for people other than the authors of the codes to use them efficiently.

There also exist several integrated packages for the calcula-

Received 16 February 2007. Accepted 6 November 2007. Published on the NRC Research Press Web site at http://cjp.nrc.ca/ on 4 June 2008.

M.F. Gu. Lawrence Livermore National Laboratory, 7000 East Avenue, Livermore, CA 94550, USA (e-mail: mfgu@ssl.berkeley.edu).

 doi: 10.1139/P07-197

tion of a variety of atomic processes, for example, the ATOM package [20], the HULLAC package [21], and the fully relativistic code (SZ) developed by Samson et al. [22] and Zhang et al. [23]. These programs treat continuum as well as bound processes. In ATOM, the radial wave functions for bound and continuum orbitals are obtained using the self-consistent field Hartree–Fock method or the frozen-core Hartree–Fock method. A relativistic version based on the Dirac equation is also available. Such a procedure tends to be very time consuming, especially for continuum processes, where the number of continuum orbitals needed is large. The HULLAC package and SZ are both based on the Dirac equation and use a single local central potential for the solution of radial orbitals. This approach is very efficient because the orthogonality of different orbitals is automatically ensured. Both programs use the distorted wave (DW) approximation for continuum processes. The difference between them is mainly in the way the local central potential is obtained. In HULLAC, a parametric potential is used and the parameters in the potential are derived by minimizing the average energies of some selected configurations [24]. In SZ, one constructs a fictitious mean configuration with fractional occupation numbers that takes into account the electron screening of all configurations involved in the physical processes to be calculated. A self-consistent Dirac–Fock–Slater iteration is then performed on this mean configuration to derive the local central potential. Although various results from these two codes have been published over the years, the programs are not available to the general public. The present package combines the strengths of these existing atomic codes, with modifications to numerical procedures to extend the capability and improve the efficiency and robustness. Although many of the techniques used in the present program were developed in existing codes, we note that FAC is written from scratch and not derived from those existing codes, such as HULLAC. The entire package is publicly available upon request to the author.

This paper reviews the theoretical background of various atomic radiative and collisional processes, the numerical techniques used for efficient computation of such data, and sample results of applications of these computational methods. Section 2 discusses the relativistic atomic structure solution and the calculation of radiative transition rates; the implementation of relativistic DW method for electron impact excitation and ionization are described in Sects. 3 and 4; Sect. 5 presents the method for computing photoionization and radiative recombination cross sections; autoionization and dielectronic recombination processes are discussed in Sect. 6; Sect. 7 introduces several example applications of the computational methods implemented in FAC; and in Sect. 8, a brief summary is given.

2. Atomic structure

The energy levels of an atomic ion with N electrons are obtained by diagonalizing the relativistic Hamiltonian H. In atomic units, which we shall use throughout the paper, it reads

$$H = \sum_{i=1}^{N} H_{\rm D}(i) + \sum_{i<j}^{N} \frac{1}{r_{ij}} \tag{1}$$

where $H_{\rm D}(i)$ is the single-electron Dirac Hamiltonian for the potential due to the nuclear charge. The basis states Φ_ν, which are usually referred to as configuration state functions (CSF), are antisymmetric sums of the products of N one-electron Dirac spinors $\varphi_{n\kappa m}$

$$\varphi_{n\kappa m} = \frac{1}{r}\begin{pmatrix} P_{n\kappa}(r)\chi_{\kappa m}(\theta,\phi,\sigma) \\ i\,Q_{n\kappa}(r)\chi_{-\kappa m}(\theta,\phi,\sigma)\end{pmatrix} \tag{2}$$

where $\chi_{\kappa m}$ is the usual spin-angular function; n is the principal quantum number; and κ is the relativistic angular quantum number, which is related to the orbital and total angular momentum through

$$\kappa = (l - j)(2j + 1) \tag{3}$$

and m is the z-component of the total angular momentum j. In coupling the angular momenta of successive shells, the standard jj coupling scheme is used.

The approximate atomic state functions are given by mixing the basis states Φ_ν with same symmetries

$$\psi = \sum_\nu b_\nu \Phi_\nu \tag{4}$$

where b_ν are the mixing coefficients obtained from diagonalizing the total Hamiltonian.

2.1. Choice of local central potential

The one-electron radial orbitals must be known to construct the Hamiltonian matrix. In the standard Dirac–Fock–Slater method, the large and small components, $P_{n\kappa}$ and $Q_{n\kappa}$, satisfy the coupled Dirac equation for a local central field $V(r)$,

$$\begin{aligned}\left(\frac{\mathrm{d}}{\mathrm{d}r} + \frac{\kappa}{r}\right) P_{n\kappa} &= \alpha\left(\varepsilon_{n\kappa} - V + \frac{2}{\alpha^2}\right) Q_{n\kappa} \\ \left(\frac{\mathrm{d}}{\mathrm{d}r} - \frac{\kappa}{r}\right) Q_{n\kappa} &= \alpha\left(-\varepsilon_{n\kappa} + V\right) P_{n\kappa}\end{aligned} \tag{5}$$

where α is the fine structure constant, and $\varepsilon_{n\kappa}$ are the energy eigenvalues of the radial orbitals.

The local central potential V includes the contribution from the nuclear charge $V^{\rm N}(r)$ and the electron–electron interaction $V^{\rm ee}(r)$. The nuclear potential can be written as

$$V^{\rm N} = \begin{cases} \frac{Z}{2}\left(\frac{r}{R_{\rm N}}\right)\left[3 - \left(\frac{r}{R_{\rm N}}\right)^2\right], & r \le R_{\rm N} \\ Z, & r > R_{\rm N}\end{cases} \tag{6}$$

where $R_{\rm N}$ is the statistical model radius of the nucleus, which can be expressed in terms of the atomic mass A, $R_{\rm N} = 2.2677 \times 10^{-5} A^{1/3}$ [25]. In the standard Dirac–Fock–Slater method, which is the approach used by SZ, the electron–electron interaction includes the spherically averaged classical potential due to the bound electrons and a local approximation to the exchange interaction,

$$\begin{aligned} V^{\rm ee}(r) &= V_{\rm c}(r) - \left[\frac{3}{4\pi^2 r^2}\sum_{n\kappa}\omega_{n\kappa}\rho_{n\kappa}(r)\right]^{1/3} \\ V_{\rm c}(r) &= \sum_{n\kappa}\int \frac{\omega_{n\kappa}}{r_>}\rho_{n\kappa}(r')\mathrm{d}r' \\ \rho_{n\kappa}(r) &= P^2_{n\kappa}(r) + Q^2_{n\kappa}(r)\end{aligned} \tag{7}$$

where $\omega_{n\kappa}$ is the occupation number of the subshell $n\kappa$, and $r_>$ is the greater of r and r'. This potential includes the undesirable self-interaction and has incorrect asymptotic behavior. In the present program, we shall use a slightly more complicated expression for $V^{\rm ee}(r)$,

$$V^{\rm ee}(r) = \frac{1}{r\sum_a \omega_a \rho_a(r)}\left\{\sum_{ab}\omega_a(\omega_b - \delta_{ab})Y^0_{bb}(r)\rho_a(r) + \sum_a \omega_a(\omega_a - 1)\sum_{k>0} f_k(a,a)Y^k_{aa}(r)\rho_a(r) + \sum_{a\neq b}\sum_k \omega_a\omega_b g_k(a,b)Y^k_{ab}(r)\rho_{ab}(r)\right\} \quad (8)$$

where $a = n\kappa$ and $b = n'\kappa'$ are the dummy indices denoting the subshells and,

$$\rho_{ab} = P_a(r)P_b(r) + Q_a(r)Q_b(r)$$
$$Y^k_{ab}(r) = r\int \frac{r^k_<}{r^{k+1}_>}\rho_{ab}(r')\mathrm{d}r' \quad (9)$$

where $r_<$ and $r_>$ are the lesser and greater of r and r', respectively. f_k and g_k are the direct and exchange coefficients defined as,

$$f_k(a,b) = -\left(1 + \frac{1}{2j_a}\right)\begin{pmatrix} j_a & k & j_b \\ -\frac{1}{2} & 0 & \frac{1}{2}\end{pmatrix}^2$$
$$g_k(a,b) = -\begin{pmatrix} j_a & k & j_b \\ -\frac{1}{2} & 0 & \frac{1}{2}\end{pmatrix}^2 \quad (10)$$

where $\begin{pmatrix} j_1 & j_2 & j_3 \\ m_1 & m_2 & m_3\end{pmatrix}$ is the Wigner $3j$ symbol. Such a choice for the electron–electron interaction is based on the fact that the quantity,

$$E^{\rm ee} = \frac{1}{2}\sum_a \omega_a < a|V^{\rm ee}|a > = \frac{1}{2}\sum_a \omega_a \int V^{\rm ee}(r)\rho_a(r)\,\mathrm{d}r \quad (11)$$

is the electron–electron contribution to the average energy of the configuration. The factor $1/2$ in (11) accounts for the double counting of electron pairs in the summation. It is easily seen that (8) has the correct asymptotic behavior at large r, since the self-interaction term is explicitly excluded.

2.2. Solution of Dirac equations

Since the potential depends on the radial orbitals sought, a self-consistent iteration is required to solve (5). In each iteration, the orbitals from the previous step are used to derive the potential. Therefore, one only needs to solve the eigenvalue problem with a known potential. As is standard, we convert (5) into a Schrödinger-like equation by eliminating the small component and performing the transformation [25],

$$P_a = \xi_a(r)F_a(r)$$
$$\xi_a(r) = \sqrt{1 + \frac{\alpha^2}{2}[\varepsilon_a - V(r)]}$$
$$Q_a = \frac{\alpha}{2\xi^2_a}\left(\frac{d}{dr}P_a + \frac{\kappa}{r}P_a\right) \quad (12)$$

Under this transformation, we have

$$\frac{\mathrm{d}^2}{\mathrm{d}r^2}F_a(r) + \left\{2[\varepsilon_a - U(r)] - \frac{\kappa(\kappa+1)}{r^2}\right\}F_a(r) = 0 \quad (13)$$

where $U(r)$ is an effective potential defined as

$$U(r) = V(r) - \frac{\alpha^2}{2}\left\{[V(r) - \varepsilon_a]^2 - W(r)\right\}$$
$$W(r) = \frac{1}{4\xi^2(r)}\left[\frac{\mathrm{d}^2}{\mathrm{d}r^2}V(r) + \frac{3\alpha^2}{4\xi^2(r)}\left(\frac{\mathrm{d}}{\mathrm{d}r}V(r)\right)^2 - \frac{2\kappa}{r}\frac{\mathrm{d}}{\mathrm{d}r}V(r)\right] \quad (14)$$

We use the standard Numerov method to solve (13). However, it is customary to perform another transformation before seeking the solution,

$$t = t(r)$$
$$F_a(r) = \left(\frac{\mathrm{d}t}{\mathrm{d}r}\right)^{-1/2}G_a(t) \quad (15)$$

where $t(r)$ as a function of radial distance is suitably chosen so that a uniform grid can be used in the new variable t, and the corresponding transformation on the wave function is to bring the differential equation for $G_a(t)$ to a Schrödinger-like form, without the first derivative term,

$$\frac{\mathrm{d}^2}{\mathrm{d}t^2}G_a(t) = \left(\frac{\mathrm{d}t}{\mathrm{d}r}\right)^{-2}G_a(t)\left\{\frac{\kappa(\kappa+1)}{r^2} - 2[\varepsilon_a - U(r)] + \frac{1}{2}\left(\frac{\mathrm{d}t}{\mathrm{d}r}\right)^{-1}\frac{\mathrm{d}^3t}{\mathrm{d}r^3} - \frac{3}{4}\left(\frac{\mathrm{d}t}{\mathrm{d}r}\right)^{-2}\left(\frac{\mathrm{d}^2t}{\mathrm{d}r^2}\right)^2\right\} \quad (16)$$

Two types of $t(r)$ have been used in the past. One is a logarithmic transformation, $t(r) \propto \ln(r)$, which has been used in the MCHF code of ref. 18; the other is a hybrid form, $t(r) = c_1 r + c_2\ln(r)$, for example, as used in ATOM [20]. The logarithmic form is not suitable for highly excited and continuum orbitals, because the radial grid interval may exceed the oscillation period of the wave function at large r. In the hybrid form, the grid interval approaches a constant at large r. For suitably chosen coefficients c_1 and c_2, it can be used in the calculation of highly excited orbitals and continua with energy below some limit. However, for free orbitals with sufficiently high energy, solving (16) in a conventional way becomes impractical. We shall use a different approach for continuum states, namely, the phase-amplitude method as used in HULLAC. For highly excited bound states, it is easily shown that the oscillation period

of the wave function is $\propto \sqrt{r}$ at large r. We, therefore, use a modified hybrid form, $t(r) = c_1\sqrt{r} + c_2 \ln(r)$, so that one oscillation period contains approximately the same number of grid points at large distances. The advantage of the modified form over the linear hybrid form is that for a given number of grid points, the modified form can cover a larger radial distance than the linear form, which is important for the calculation of highly excited states.

The minimum and maximum radial distances, $r_{\min}$ and $r_{\max}$, in setting up the radial grid are chosen as,

$$\begin{aligned} r_{\min} &= 10^{-6}/Z_{\text{eff}} \\ r_{\max} &= 500/Z_{\text{eff}} \end{aligned} \tag{17}$$

where Z_{eff} is the residual charge of the atomic ion that the electrons experience at large r. This ensures that $r_{\min}$ is well within the nuclear charge distribution for any atomic system. The value of $r_{\max}$ ensures that for excited states below $n \sim 20$, the bound energies are less than the Coulomb potential at $r_{\max}$. These states have no nodes at $r > r_{\max}$. For states with higher n, however, wave functions beyond $r_{\max}$ may have additional nodes. Therefore, counting the nodes is no longer a valid method for selecting the right solution. Moreover, the wave functions can no longer be normalized by calculating their norm with simple numerical integration, since the contributions beyond $r_{\max}$ cannot be neglected. One may increase $r_{\max}$ when highly excited states are needed. One must also increase the number of grid points to ensure the accuracy of numerical integration. However, wave functions at large radial distances are rarely needed either because the interaction operators are negligible or because the states that interact with such highly excited orbitals have negligible amplitudes at large distances. In the present program, the low-n and high-n states are treated differently. The dividing n_0 is determined by the choice of $r_{\max}$, specifically, $n_0 = 0.5\sqrt{Z_{\text{eff}} r_{\max}}$. For $n \le n_0$, the orbitals are found by outward and inward integration of (16) with zero amplitudes at both ends and matching at the outer classical turning point. Node counting is used to pick out the appropriate solution corresponding to the quantum numbers n and l. The wave functions are then normalized by numerical integration. For $n > n_0$, (16) is integrated outward until $r = r_{\text{core}}$, where the potential has reached its asymptotic Coulomb value. For $r > r_{\text{core}}$, the wave function is the regular Dirac–Coulomb function with an appropriate quantum defect [26]. The quantum defect and normalization of the wave function is determined by matching the numerical solution inside r_{core} to that of the Dirac–Coulomb function at r_{core}.

2.3. Angular integration and the Hamiltonian matrix elements

In (1), the first term of the Hamiltonian is a one-electron operator, while the second term is a two-electron operator. The traditional method of evaluating their matrix elements is to expand them into a sum, with each term being a product of an angular part and a radial part. The angular part is then calculated using Racah algebra. In doing so, the initial and final basis states need to be recoupled, which is often carried out by the recoupling program of Grant [27]. Recently, Gaigalas et al. [28] proposed a new method of performing angular integration that is based on the second quantization form of the operators and extends the use of Racah algebra to the quasi-spin space. In this method, instead of recoupling basis states, one recouples the creation and annihilation operators with the help of Racah algebra. The main advantage of this method is that there are only two creation and two annihilation operators in the two-electron interaction, while for the one-electron interaction, there is only one creation and one annihilation operator. Therefore, at most four angular momenta are involved in the recoupling, independent of the shell structure of the basis states. In the conventional method, the recoupling of basis states can be quite complicated for complex configurations. The present code adopts the new method and the program of Gaigalas et al. [29] is used for the reduced matrix elements of creation and annihilation operators.

2.3.1. One-electron operators

The one-electron operator in the Hamiltonian is a scalar, however, we treat a general tensorial operator $O^L_M = \sum_i o^L_M(i)$ in this section since the calculation of radiative transition rates involves tensors. In second quantization form, O^L_M may be expressed as

$$O^L_M = \sum_{\hat{\alpha}\hat{\beta}} a^\dagger_{\hat{\alpha}} a_{\hat{\beta}} < \hat{\alpha}|o^L_M|\hat{\beta} > \tag{18}$$

where $\hat{\alpha}$ and $\hat{\beta}$ denote a single electron state $n\kappa m$. $a^\dagger$ is the creation operator and a is the annihilation operator. Using the Wigner–Ekart theorem for the matrix elements of o^L_M we have,

$$O^L_M = \sum_{\alpha\beta} Z^L_M(\alpha, \beta) < \alpha||o^L||\beta > \tag{19}$$

where $< \alpha||o^L||\beta >$ denotes the reduced matrix element, and α and β denote only quantum numbers $n\kappa$. The summation over m is already contained in Z^L_M, which is defined as,

$$Z^L_M(\alpha, \beta) = -[L]^{-1/2} \left[a^\dagger_{\hat{\alpha}} \times \tilde{a}_{\hat{\beta}}\right]^L_M \tag{20}$$

where $[L] = 2L + 1$, and $\tilde{a}_{\hat{\beta}} = (-1)^{j_\beta - m_\beta} a_{-\hat{\beta}}$ with $-\hat{\beta}$ being understood as the single electron state $n_\beta \kappa_\beta - m_\beta$, i.e., having the magnetic quantum number negated. Such a transformation is necessary since it is $\tilde{a}_{\hat{\beta}}$ that form an irreducible tensorial set with rank j_β [30]. The tensorial coupling has the usual meaning. The angular integration is equivalent to the evaluation of the reduced matrix elements of Z^L_M between basis states [28].

2.3.2. Two-electron operators

After some algebraic manipulation [31], the electrostatic interaction between electrons can be written as,

$$\sum_{i<j} \frac{1}{r_{ij}} = \frac{1}{2} \sum_{\alpha\beta\gamma\delta} \sum_k \Big\{ Z^k(\alpha, \gamma) \cdot Z^k(\beta, \delta) - (-1)^{j_\alpha - j_\beta} [j_\alpha]^{-1/2} Z^0_0(\alpha\delta) \Big\} X^k(\alpha\beta; \gamma\delta) \tag{21}$$

where $Z^k(\alpha, \gamma) \cdot Z^k(\beta, \delta)$ denotes the scalar product of the two tensors, and

$$X^k(\alpha\beta; \gamma\delta) = < \alpha||C^k||\gamma >< \beta||C^k||\delta > R^k(\alpha\beta; \gamma\delta) \tag{22}$$

where C^k is the normalized spherical harmonic tensor as defined in ref. 17, and R^k is the generalized Slater integral,

$$R^k(\alpha\beta;\,\gamma\delta) = \int \frac{r_<^k}{r_>^{k+1}} \rho_{\alpha\gamma}(r_1)\rho_{\beta\delta}(r_2)\,\mathrm{d}r_1\,\mathrm{d}r_2 \tag{23}$$

The calculation of the matrix elements of $Z^k(\alpha,\gamma)\cdot Z^k(\beta,\delta)$ follows ref. 28.

2.4. Radiative transition rates

The radiative transition rates are calculated in the single multipole approximation. This means that the interference between different multipoles is not taken into account, although rates corresponding to arbitrary multipoles can be calculated. For a given multipole operator O_M^L and initial and final states of the transition $\psi_i = \sum_v b_{iv}\Phi_v$ and $\psi_f = \sum_\mu b_{f\mu}\Phi_\mu$, the line strength of the transition is

$$\begin{aligned} S_{fi} &= \left| < \psi_f || O_M^L || \psi_i > \right|^2 \\ &= \left| \sum_{\mu v} b_{f\mu} b_{iv} \sum_{\alpha\beta} < \Phi_\mu || Z_M^L(\alpha,\beta) || \Phi_v > \right. \\ &\qquad \left. < \alpha || C^L || \beta > M_{\alpha\beta}^L \right|^2 \end{aligned} \tag{24}$$

where $M_{\alpha\beta}^L$ is the radial part of the single-electron multipole operator as defined in ref. 32. The weighted oscillator strength and transition rates are given by,

$$gf_{\mathrm{fi}} = [L]^{-1}\omega(\alpha\omega)^{2L-2}S_{\mathrm{fi}} \tag{25}$$

$$gA_{\mathrm{fi}} = 2\alpha^3\omega^2 gf_{\mathrm{fi}} \tag{26}$$

where $\omega = E_{\mathrm{i}} - E_{\mathrm{f}}$ is the transition energy.

$M_{\alpha\beta}^L$ may be calculated using the fully relativistic expressions of ref. 32. However, in most cases (except for M1 transitions, where the use of the fully relativistic expressions is essential), their nonrelativistic limits are sufficiently accurate, which has the advantage that these operators depend on the transition energy in a trivial manner.

3. Electron impact excitation

Two classes of methods are commonly used in the calculation of electron impact excitation (EIE) cross sections. The first is based on a set of close-coupling (CC) equations, which takes into account the coupling of various excitation channels [33]. In these methods, resonances can be included in a natural way by including the coupling to closed channels. Several implementations of this method exist. The most widely used is the R-matrix code developed by a group at the Queens University of Belfast [34]. The second class of methods is based on the first-order Born approximation, which assumes independent excitation channels. The coupling to closed channels, which results in resonances, may be included with perturbation methods [35]. Different variants exist according to the different treatments of the continuum wave functions. The plane-wave (PW) Born approximation uses an unperturbed plane wave for the free orbital. The Coulomb-wave (CW) Born approximation takes into account the distortion of the continuum due to a pure Coulomb potential. The most accurate of this class is the DW Born approximation, in which the free orbitals are calculated in a more realistic potential taking into account the electronic structure of the target ion. The majority of the computer programs in this class implement the DW approximation, since it yields significantly better results than the PW and CW methods with minimal increase in complexity. Many DW codes are in use today. For example, the nonrelativistic DW code from University College London [36], the relativistic code of Hagelstein and Jung [37], the HULLAC package [31], the code by Zhang et al. [23], and that of Chen [38], just to name a few. The present DW implementation in FAC is, in principle, similar to any of the relativistic codes listed above.

3.1. Factorized collision strength

The EIE cross section σ_{01} from the initial state ψ_0 to the final state ψ_1 can be expressed in terms of the collision strength Ω_{01} as,

$$\sigma_{01} = \frac{\pi}{k_0^2 g_0}\Omega_{01} \tag{27}$$

where g_0 is the statistical weight of the initial state, and k_0 is the kinetic momentum of the incident electron, which is related to the energy ε_0 by,

$$k_0^2 = 2\varepsilon_0\left(1 + \frac{\alpha^2}{2}\varepsilon_0\right) \tag{28}$$

where α is the fine structure constant. The continuum wavefunction is normalized so that the large component has an asymptotic amplitude of $\sqrt{k/\varepsilon}$, which reduces to $\sqrt{2/k}$ in the nonrelativistic limit, or equivalently,

$$\int_0^\infty \left[P_{\varepsilon(r)}P_{\varepsilon'}(r) + Q_{\varepsilon(r)}Q_{\varepsilon'}(r)\right]\mathrm{d}r = \pi\delta(\varepsilon - \varepsilon') \tag{29}$$

where ε and k are the energy and kinetic momentum of the orbital, and P_ε and Q_ε are the large and small components of the continuum wave function. The collision strength can be written as,

$$\begin{aligned} \Omega_{01} = 2\sum_{\kappa_0\kappa_1}\sum_{J_{\mathrm{T}}}[J_{\mathrm{T}}] &\left| < \psi_0\kappa_0,\, J_{\mathrm{T}}M_{\mathrm{T}} \right| \\ &\left. \sum_{i<j}\frac{1}{r_{ij}} \left| \psi_1\kappa_1,\, J_{\mathrm{T}}M_{\mathrm{T}} > \right|^2 \right. \end{aligned} \tag{30}$$

where κ_0 and κ_1 are the relativistic angular quantum numbers of the incident and scattered electrons, J_{T} is the total angular momentum when the target state is coupled to the continuum orbital, M_{T} is the projection of the total angular momentum, and $[J] = 2J + 1$. Following ref. 31, this expression can be simplified to give,

$$\begin{aligned} \Omega_{01} = 2\sum_k \sum_{\substack{\alpha_0\alpha_1 \\ \beta_0\beta_1}} Q^k(\alpha_0\alpha_1;\,\beta_0\beta_1) &< \psi_0 || Z^k(\alpha_0,\alpha_1) || \psi_1 > \\ &< \psi_0 || Z^k(\beta_0,\beta_1) || \psi_1 > \end{aligned} \tag{31}$$

where

$$Q^k(\alpha_0\alpha_1;\,\beta_0\beta_1) = \sum_{\kappa_0\kappa_1}[k]^{-1}\,P^k(\kappa_0\kappa_1;\,\alpha_0\alpha_1)\,P^k(\kappa_0\kappa_1;\,\beta_0\beta_1) \quad (32)$$

and

$$P^k(\kappa_0\kappa_1;\,\alpha_0\alpha_1) = X^k(\alpha_0\kappa_0;\,\alpha_1\kappa_1) + \sum_t(-1)^{k+t}[k]\begin{Bmatrix} j_{\alpha_0} & j_1 & t \\ j_0 & j_{\alpha_1} & k\end{Bmatrix} X^t(\alpha_0\kappa_0;\,\kappa_1\alpha_1) \quad (33)$$

where X^k and the operator $Z^k(\alpha,\,\beta)$ are defined in Sect. 2.

The importance of (31) is that the angular and radial integrals are completely factorized. The radial integrals $Q^k(\alpha_0\alpha_1;\,\beta_0\beta_1)$ with the same set of bound orbitals α_0, α_1, β_0, and β_1 may appear in many transitions. These integrals also depend on the energy of incident and scattered electrons, or for a fixed scattered electron energy, they depend on the excitation energy of the transition ΔE. However, as noted in ref. 31, the dependence on ΔE is rather weak. For dipole forbidden radial integrals, $Q^k \propto \Delta E$, and for dipole allowed integrals, $Q^k \propto \ln \Delta E$ approximately holds over a wide range of transition energies. Therefore, for a given scattered electron energy, Q^k may be calculated at a few values of ΔE, and the integral at the actual transition energy can be interpolated from these few values. In practice, usually a three-point grid spanning the entire transition energy range for a given array of excitations yields sufficiently accurate results. The dependence of Q^k on ε_1, the scattered electron energy, although not as simple as that on ΔE, is still rather smooth and has known asymptotic behavior at large energies according to the type of the transition. We use interpolation on ε_1 as well with a few more points. The calculation of $< \psi_0||Z^k||\psi_1 >$ is the same as that involved in the radiative transition rates.

3.2. Solution of the Dirac equation for the continuum

In FAC, the continuum orbitals are obtained by solving the Dirac equations with the same central potential as that for bound orbitals. However, in obtaining the potential one may optionally add a high-lying subshell to the mean configuration to account for the fact that the continuum wave functions experience the screening of one additional electron at large distances. Such a high-lying subshell has little effect on the bound orbitals because the deviation of the potential from its correct asymptotic value starts at a very large distance where the bound orbitals have exponentially decayed. After transforming the Dirac equations to a second-order Schrödinger-like equation and adopting the same radial grid as in the solution of bound orbitals, the transformed large component, $F(r)$, of the free orbital satisfies (13), except that the boundary condition at infinity is replaced by the requirement that the original large component $P(r)$ has the asymptotic amplitude of $\sqrt{k/\varepsilon}$.

In solving (13), the radial grid is divided into two regions. In the inner region, where the wave function is not oscillatory, or the oscillation period is large enough to contain a sufficient number of grid intervals (for example, more than 16), we use the standard Numerov method to integrate the equation outward. Beyond some point $r = r_c$, which depends on the energy and angular momentum of the continuum sought, the oscillation period of the wave function becomes too small for the direct integration to be accurate. At that point, we switch to a phase-amplitude method, in which $F(r)$ is written as,

$$F(r) = A\frac{1}{\eta^{1/2}(r)}\sin\phi(r) \quad (34)$$

where the constant A is chosen to ensure the appropriate normalization. $\phi(r)$ and $\eta(r)$ satisfy,

$$\phi(r) = \int_0^r \eta(s)\,\mathrm{d}s$$
$$\eta^2(r) = \eta^{1/2}\frac{\mathrm{d}^2}{\mathrm{d}r^2}\eta^{-1/2} + \omega^2(r) \quad (35)$$

where

$$\omega^2(r) = 2\,[\varepsilon - U(r)] - \frac{\kappa(\kappa+1)}{r^2} \quad (36)$$

For $r > r_c$, (35) can be easily solved by iteration starting from the first-order WKB approximation $\eta(r) = \omega(r)$. In fact, in most cases, the first-order approximation itself is sufficiently accurate. The inner and outer solutions are matched at r_c by requiring the continuity of $F(r)$ and its first derivative.

3.3. Evaluation of radial integrals

The evaluation of Slater integrals reduces to the calculation of the following type of integrals,

$$I = \int_0^\infty P_a(r)\,f(r)\,P_b(r)\,\mathrm{d}r \quad (37)$$

where $P_a(r)$ and $P_b(r)$ may be large or small components of either bound or continuum orbitals, and $f(r)$ is a smooth function of r. If both wave functions are from bound orbitals, direct numerical integration is used.

If one of them is from a continuum orbital, we divide the integration range into two regions. In the first region, $r < r_c$, the integration proceeds as in the bound–bound case. In the $r > r_c$ region, the integral is of the type,

$$I_1 = \int g(r)\sin\phi(r)\,\mathrm{d}r \quad (38)$$

or

$$I_2 = \int g(r)\cos\phi(r)\,\mathrm{d}r \quad (39)$$

where $g(r)$ is a smooth function of r. Since the phase ϕ is also a smooth function of r, we evaluate I_1 as,

$$I_1 = \int \tilde{g}(\phi)\sin\phi\,\mathrm{d}\phi \quad (40)$$

where

$$\tilde{g}(\phi) = g(r)\frac{\mathrm{d}r}{\mathrm{d}\phi} \quad (41)$$

which is a smooth function of ϕ. Using its values at each grid point, it is represented by a cubic spline interpolation function. Therefore, within each grid interval it is a third-order polynomial of ϕ. I_1 is evaluated by integrating $\int \phi^n \sin\phi d\phi$ analytically, where $n = 0$, 1, 2, or 3. The evaluation of I_2 is similar, replacing $\sin\phi$ with $\cos\phi$.

If both wave functions are from the continuum, the integration range is divided into three regions. In the first region, $r < \min(r_{c1}, r_{c2})$, the integration proceeds as in the bound–bound case. In the second region, $\min(r_{c1}, r_{c2}) < r < \max(r_{c1}, r_{c2})$, the integration proceeds as in the bound-free case. In the last region, $r > \max(r_{c1}, r_{c2})$, both wave functions are in the phase-amplitude form, the integrals are of the type,

$$I = \int g(r) \sin\phi_1(r) \sin\phi_2(r)\, \mathrm{d}r \tag{42}$$

or similar ones where one or both sine functions are replaced by cosine functions. Such integrals are transformed to the sum of two terms,

$$I^+ = \int g^+(r) \cos\phi^+(r)\, \mathrm{d}r$$
$$I^- = \int g^-(r) \cos\phi^-(r)\, \mathrm{d}r \tag{43}$$

or variants where the cosine function is replaced by the sine function. In the above equation, $\phi^+ = \phi_1 + \phi_2$ and $\phi^- = \phi_1 - \phi_2$, respectively. These integrals are evaluated similarly to the bound-free integrals except when the energies of two continuum orbitals are very close so that ϕ^- is very small, in which case the integrals containing ϕ^- are calculated directly in the radial variable r.

3.4. Magnetic sublevel excitation

In many cases, only the total excitation cross sections are of importance, at least when the electron distribution functions are isotropic. However, there exist situations where aligned excitation produces polarized line emission. Suggestions have been made to use such polarized light to study beam–plasma interactions in solar flares [39, 40] and the properties of tokamak plasmas [41]. Line polarization is also an important factor to take into account in the analysis of laboratory spectroscopic data involving a directional electron beam, such as electron beam ion traps [42, 43].

To determine the degree of polarization and angular distribution of emitted lines driven by electron collisional excitation, one needs detailed cross sections between the magnetic sublevels of lower and upper states. Several authors have made calculations of such cross sections involving magnetic sublevels. For example, Inal and Dubau [44] made DW calculations using nonrelativistic radial wave functions, but they included intermediate-coupling effects by transforming the reactance matrices from LS-coupling to a relativistic pair-coupling scheme. Zhang et al. [45] performed the first fully relativistic DW calculations of magnetic sublevel collision strengths with a modified version of their previous program for total cross sections.

In FAC, we have generalized the factorization theory of EIE discussed earlier to the excitation of magnetic sublevels by a unidirectional electron beam. We start from the scattering amplitude $B^{m_{sf}}_{m_{si}}$ given in ref. 45,

$$B^{m_{sf}}_{m_{si}} = \frac{2\pi}{k_i} \sum_{\substack{l_i,m_{li},j_i,m_i \\ l_f,m_{lf},j_f,m_f}} (i)^{l_i-l_f+1} \exp\left[i(\delta_i+\delta_f)\right] Y^{m_{li}*}_{l_i}\left(\hat{\mathbf{k}}_i\right) Y^{m_{lf}}_{l_f}\left(\hat{\mathbf{k}}_f\right) C\left(l_i \frac{1}{2} m_{li} m_{si};\, j_i m_i\right) \times C\left(l_f \frac{1}{2} m_{lf} m_{sf};\, j_f m_f\right) T\left(\alpha_i, \alpha_f\right) \tag{44}$$

where $T(\alpha_i, \alpha_f)$ are the transition matrix elements in the representation where the free electrons are uncoupled to the targets, and $C(lsm_l m_s;\, jm)$ represents the Clebsch–Gordan coefficient. The uncoupled state is

$$\alpha_i = k_i \tilde{j}_i m_i J_i M_i, \qquad \alpha_f = k_f \tilde{j}_f m_f J_f M_f \tag{45}$$

where $\tilde{j}$ denotes $\{l, j\}$. The differential cross section is

$$\frac{\mathrm{d}\sigma}{\mathrm{d}\hat{k}_f} = \left| B^{m_{sf}}_{m_{si}} \right|^2 \tag{46}$$

Choosing the direction of the incident electron as the z axis, integrating over $\hat{k}_f$, summing over m_{sf}, and averaging over m_{si} gives,

$$\sigma(J_f M_f, J_i M_i) = \frac{\pi}{2k_i^2} \sum_{\substack{\tilde{j}_i,\tilde{j}'_i,\tilde{j}_f \\ m_{si},m_f}} (i)^{l_i-l'_i} \exp[i(\delta_i - \delta_{i'})] ([l_i][l'_i])^{1/2} (-1)^{j_i+j'_i+2m_i} ([j_i][j'_i])^{1/2} \begin{pmatrix} j_i & \frac{1}{2} & l_i \\ -m_i & m_{si} & 0 \end{pmatrix} \begin{pmatrix} j'_i & \frac{1}{2} & l'_i \\ -m_i & m_{si} & 0 \end{pmatrix} \times T(\alpha_i, \alpha_f) T^*(\alpha'_i, \alpha_f) \tag{47}$$

In the first-order perturbation theory,

$$T(\alpha_i,\alpha_f)=-2i\sum_t\sum_{\substack{\tilde{j}_i j_0\\ \tilde{j}_f j_1}} < J_iM_i\tilde{j}_im_i|Z^t(j_0,j_1)\cdot Z^t(\tilde{j}_i,\tilde{j}_f)|J_fM_f\tilde{j}_fm_f > P^t(\tilde{j}_i\tilde{j}_f;j_0j_1) \tag{48}$$

where $P^t(\tilde{j}_i\tilde{j}_f;j_0j_1)$ is defined by (33). Substituting this expression into (47),

$$\begin{aligned}\sigma(J_fM_f,J_iM_i)=\frac{2\pi}{k_i^2}\sum_{\substack{\tilde{j}_i,\tilde{j}_i',\tilde{j}_f\\ m_{si},m_f}}\sum_{\substack{j_0,j_1\\ j_0',j_1'}}\sum_{t,t'}(i)^{l_i-l_i'}\exp[i(\delta_i-\delta_{i'})]([l_i][l_i'])^{1/2}\times(-1)^{j_i+j_i'+2m_i}([j_i][j_i'])^{1/2}\\ \begin{pmatrix} j_i & \frac{1}{2} & l_i\\ -m_i & m_{si} & 0\end{pmatrix}\begin{pmatrix} j_i' & \frac{1}{2} & l_i'\\ -m_i & m_{si} & 0\end{pmatrix}\times\left\langle J_iM_i\tilde{j}_im_i\left|Z^t(j_0j_1)\cdot Z^t(\tilde{j}_i\tilde{j}_f)\right|J_fM_f\tilde{j}_fm_f\right\rangle\\ \times\left\langle J_iM_i\tilde{j}_i'm_i\left|Z^{t'}(j_0'j_1')\cdot Z^{t'}(\tilde{j}_i'\tilde{j}_f)\right|J_fM_f\tilde{j}_fm_f\right\rangle\times P^t(\tilde{j}_i\tilde{j}_f;j_0j_1)P^{t'}(\tilde{j}_i'\tilde{j}_f;j_0'j_1')\end{aligned} \tag{49}$$

Expanding the scalar product in the spherical tensors, we have,

$$\begin{aligned}\left\langle J_iM_i\tilde{j}_im_i\left|Z^t(j_0j_1)\cdot Z^t(\tilde{j}_i\tilde{j}_f)\right|J_fM_f\tilde{j}_fm_f\right\rangle&=\sum_q(-1)^q < \tilde{j}_im_i|z^t_{-q}(\tilde{j}_f\tilde{j}_f)|\tilde{j}_im_i > \times < J_iM_i|Z^t_q(j_0j_1)|J_fM_f >\\ &=(-1)^{q+j_i-m_i+J_i-M_i}\begin{pmatrix} j_i & t & j_f\\ -m_i & -q & m_f\end{pmatrix}\begin{pmatrix} J_i & t & J_f\\ -M_i & q & M_f\end{pmatrix}\langle J_iM_i\,||Z^t(j_0j_1)||\,J_fM_f\rangle\end{aligned} \tag{50}$$

The summation over q may be dropped since it is fixed by the $3j$ symbols to be M_i-M_f. Therefore,

$$\begin{aligned}\sigma(J_fM_f,J_iM_i)=\frac{2\pi}{k_i^2}\sum_{tt'}\begin{pmatrix} J_i & t & J_f\\ -M_i & q & M_f\end{pmatrix}\begin{pmatrix} J_i & t' & J_f\\ -M_i & q' & M_f\end{pmatrix}\sum_{\substack{j_0j_1\\ j_0'j_1'}}\langle J_iM_i\,||Z^t(j_0j_1)||\,J_fM_f\rangle\left\langle J_iM_i\left|\left|Z^{t'}(j_0'j_1')\right|\right|J_fM_f\right\rangle\\ \times\sum_{\substack{\tilde{j}_i,\tilde{j}_i',\tilde{j}_f\\ m_{si},m_f}}(i)^{l_i-l_i'}\exp[i(\delta_i-\delta_{i'})]([l_i][l_i'])^{1/2}\times([j_i][j_i'])^{1/2}\begin{pmatrix} j_i & \frac{1}{2} & l_i\\ -m_i & m_{si} & 0\end{pmatrix}\begin{pmatrix} j_i' & \frac{1}{2} & l_i'\\ -m_i & m_{si} & 0\end{pmatrix}\\ \times\begin{pmatrix} j_i & t & j_f\\ -m_i & -q & m_f\end{pmatrix}\begin{pmatrix} j_i' & t' & j_f\\ -m_i & -q' & m_f\end{pmatrix}\times P^t(\tilde{j}_i\tilde{j}_f;j_0j_1)P^{t'}(\tilde{j}_i'\tilde{j}_f;j_0'j_1')\end{aligned} \tag{51}$$

or it may be written as,

$$\sigma(J_fM_f,J_iM_i)=\frac{2\pi}{k_i^2}\sum_{tt'}\begin{pmatrix} J_i & t & J_f\\ -M_i & q & M_f\end{pmatrix}\begin{pmatrix} J_i & t' & J_f\\ -M_i & q' & M_f\end{pmatrix}\sum_{\substack{j_0j_1\\ j_0'j_1'}}A^t(j_0j_1)A^{t'}(j_0'j_1')Q^{tt'}(j_0j_1,j_0'j_1') \tag{52}$$

with

$$A^t(j_0j_1)=\langle J_iM_i\,||Z^t(j_0j_1)||\,J_fM_f\rangle \tag{53}$$

and

$$\begin{aligned}Q^{tt'}(j_0j_1,j_0'j_1')=\sum_{\substack{\tilde{j}_i,\tilde{j}_i',\tilde{j}_f\\ m_{si},m_f}}(i)^{l_i-l_i'}\exp[i(\delta_i-\delta_{i'})]([l_i][l_i'])^{1/2}\times([j_i][j_i'])^{1/2}\begin{pmatrix} j_i & \frac{1}{2} & l_i\\ -m_i & m_{si} & 0\end{pmatrix}\begin{pmatrix} j_i' & \frac{1}{2} & l_i'\\ -m_i & m_{si} & 0\end{pmatrix}\\ \times\begin{pmatrix} j_i & t & j_f\\ -m_i & -q & m_f\end{pmatrix}\begin{pmatrix} j_i' & t' & j_f\\ -m_i & -q' & m_f\end{pmatrix}P^t(\tilde{j}_i\tilde{j}_f;j_0j_1)P^{t'}(\tilde{j}_i'\tilde{j}_f;j_0'j_1')\end{aligned} \tag{54}$$

In (51), after summation over M_f and averaging over M_i, the first two $3j$ symbols produce $\delta_{tt'}\delta_{qq'}$, then the summation over m_f and q in the last two $3j$ symbols gives $\delta_{j_ij_i'}$, and finally the summation over m_{si} and m_i gives $\delta_{l_il_i'}$, which cancels the phase factors, and we recover the factorization formula for the total cross section. Just as the formula for the total cross section, (51) also completely factorizes the angular and radial integrals, and similar interpolation procedures for the radial integrals can be applied.

4. Electron impact ionization

4.1. Relativistic distorted wave theory

The formula for the DW electron impact ionization (EII) cross section differential in energy of the ejected electron, may be obtained from that for EIE by replacing one bound orbital in the final state with the free orbital of the ejected electron and summing over its angular momentum. It can be expressed in terms of the collision strength similar to that of EIE,

$$\sigma(\varepsilon_0, \varepsilon) = \frac{1}{k_0^2 g_0}\Omega_{01} \tag{55}$$

where ε_0 and k_0 are the energy and kinetic momentum of the incident electron, and ε is the energy of the ejected electron. The normalization of continuum orbitals is discussed in Sect. 3. Note that the absence of the factor π, compared with the formula for the EIE cross section, is due to the different normalization of the free and bound orbitals. The collision strength Ω_{01} is

$$\Omega_{01} = 2\sum_{\substack{\kappa, J_T \\ k, \alpha_0\beta_0}} Q^k(\alpha_0\kappa; \beta_0\kappa) < \psi_0||Z^k(\alpha_0, \kappa)||\psi_1, \kappa; J_T >< \psi_0||Z^k(\beta_0, \kappa)||\psi_1, \kappa; J_T > \tag{56}$$

where κ is the relativistic angular quantum number of the ejected electron, J_T is the total angular momentum of the final state coupled with the ejected electron, the radial part Q^k is identical to that for EIE, except that one of the bound orbitals in the final state is now replaced by a free orbital. Note that Q^k contains the summation over the partial waves of incident and scattered electrons.

The angular factors involving the free electron can be simplified using the decoupling formula of Racah,

$$\sum_{J_T} < \psi_0||Z^k(\alpha_0, \kappa)||\psi_1, \kappa; J_T >< \psi_0||Z^k(\beta_0, \kappa)||\psi_1, \kappa; J_T >=$$
$$(-1)^{j_{\alpha_0} - j_{\beta_0}} < \psi_1||\tilde{a}_{\tilde{\alpha_0}}||\psi_0 >< \psi_1||\tilde{a}_{\tilde{\beta}_0}||\psi_0 > \sum_{J_T}[J_T] \begin{Bmatrix} J_1 & j & J_T \\ k & J_0 & j_{\alpha_0} \end{Bmatrix} \begin{Bmatrix} J_1 & j & J_T \\ k & J_0 & j_{\beta_0} \end{Bmatrix} \tag{57}$$

where $[J_T]$ denotes $2J_T + 1$ and $\begin{Bmatrix} j_1 & j_2 & j_3 \\ j_4 & j_5 & j_6 \end{Bmatrix}$ is the Wigner $6j$ symbol. Substituting this into (56) and after carrying out the summation over J_T analytically, we find,

$$\Omega_{01} = 2\sum_{k, \alpha_0\beta_0} \delta_{j_{\alpha_0} j_{\beta_0}} [j_{\alpha_0}]^{-1} \overline{Q}^k(\alpha_0, \beta_0) < \psi_1||\tilde{a}_{\tilde{\alpha_0}}||\psi_0 >< \psi_1||\tilde{a}_{\tilde{\beta}_0}||\psi_0 > \tag{58}$$

where $\overline{Q}^k(\alpha_0, \beta_0) = \sum_\kappa Q^k(\alpha_0\kappa; \beta_0\kappa)$. Note that since only basis states with the same parity can mix, the condition $j_{\alpha_0} = j_{\beta_0}$ implies that $l_{\alpha_0} = l_{\beta_0}$ as well. Therefore, if the configuration interaction is limited within the same n complex, only terms with $\alpha_0 = \beta_0$ survive in the summation.

The total ionization cross section is obtained by integrating Ω_{01} over the energy of the ejected electron ε,

$$\sigma(\varepsilon_0) = \int_0^{(\varepsilon_0 - I)/2} \sigma(\varepsilon_0, \varepsilon)\, \mathrm{d}\varepsilon \tag{59}$$

where I is the ionization energy. The ionization energy enters the radial integral Q^k implicitly, since $\varepsilon_0 = I + \varepsilon_1 + \varepsilon$, where ε_1 is the energy of the scattered electron.

4.2. Coulomb–Born-exchange approximation

The computation of radial integrals in the DW approximation is relatively time consuming. In many applications, fast and less accurate methods are highly desirable. The Coulomb–Born-exchange (CBE) approximation implemented in the present program is one of such methods. In this method, we only retain terms with $\alpha_0 = \beta_0$ in (58). After the integration over the energy of the ejected electron, a reduced radial integral is defined as,

$$Q_R(\alpha_0) = I_{\alpha_0} I \sum_k \int_0^{(\varepsilon_0 - I)/2} \overline{Q}^k(\alpha_0, \alpha_0)\, \mathrm{d}\varepsilon \tag{60}$$

where I_{α_0} is the binding energy of the orbital α_0. It is well known that the reduced radial integrals are not very sensitive to the difference in the electronic structures and nuclear charges [46]. We therefore use the hydrogenic values, calculated under the CBE approximation [47, 48], in place of detailed DW radial integrals. A simple parameterized formula as given in ref. 46 is used for this purpose.

$$Q_R = A\ln(u) + D\left(1 - \frac{1}{u}\right)^2 + \left(\frac{c}{u} + \frac{\mathrm{d}}{u^2}\right)\left(1 - \frac{1}{u}\right) \tag{61}$$

where $u = \varepsilon_0/I$. In fact, even in the detailed DW calculations, the computed radial integrals are fitted with this formula, fixing the coefficient A according to the correct Bethe limit. The parameters are then used to obtain total ionization cross sections at many incident energies. It is also possible to use the parameters given by ref. 49 instead of the CBE values to bring the results into better agreement with the detailed DW calculations.

4.3. Binary-encounter-dipole theory

The CBE approximation discussed earlier attempts to capture the detail of the ionic structure through a universal reduced

radial integral. In the binary-encounter-dipole (BED) theory developed by Kim and Rudd [50], a semi-empirical formula for the radial integrals is derived by combining the Mott cross section and binary encounter cross section, taking into account the high-energy Bethe limit. The computation of bound-free differential oscillator strengths (discussed in Sect. 5), which are related to the Bethe coefficients, is much simpler than the DW calculation of ionization radial integrals. Therefore, the BED implementation is very efficient in practice. A unique feature of the BED theory is the energy denominator $\varepsilon_0 + I$ (for neutral atoms, the average kinetic energy of the active bound electron should also be added), as opposed to ε_0 in various first-order Born approximations (including DW). This modification effectively introduces a scaling factor $\varepsilon_0/(\varepsilon_0 + I)$, which reduces the ionization cross sections at low energies. Comparison with experimental results for low-Z near neutral ions indicates that such scaling brings the theoretical results into better agreement with experiment [50]. However, for highly charged ions, we find that this scaling reduces the cross -sections by a too large factor. A modified scaling factor is therefore introduced as $\varepsilon_0/(\varepsilon_0 + I_s)$ with,

$$I_s = \frac{N}{2Z - N} I \tag{62}$$

where N is the number of electrons of the ion and Z is the atomic number.

5. Photoionization and radiative recombination

5.1. Factorized formula for cross sections

The partial photoionization (PI) cross section can be expressed in terms of the differential oscillator strength (in atomic units), and the partial radiative recombination (RR) cross section is related to that of PI through the Milne relation,

$$\sigma_{\rm PI} = 2\pi\alpha \frac{{\rm d}f}{{\rm d}E}$$
$$\sigma_{\rm RR} = \frac{\alpha^2}{2} \frac{g_{\rm i}}{g_{\rm f}} \frac{\omega^2}{\varepsilon(1 + 0.5\alpha^2\varepsilon)} \sigma_{\rm PI} \tag{63}$$

where α is the fine structure constant, $g_{\rm i}$ and $g_{\rm f}$ are the statistical weight of the bound states before and after the photoionzation takes place, respectively, ω is the photon energy, and ε is the energy of the ejected photo-electron. The differential oscillator strength, ${\rm d}f/{\rm d}E$, may be calculated similar to the bound–bound oscillator strength through the generalized line strength,

$$\frac{{\rm d}f}{\rm d} = \frac{\omega}{g_{\rm i}} [L]^{-1} (\alpha\omega)^{2L-2} S \tag{64}$$

where L is the rank of the multipole operator inducing the transition, $[L]$ denotes $2L + 1$, and the generalized line strength is

$$S = \sum_{\kappa J_{\rm T}} \left| < \psi_{\rm f}, \kappa; J_{\rm T} || O^L || \psi_i > \right|^2 \tag{65}$$

where κ is the relativistic quantum number of the free electron, $J_{\rm T}$ is the total angular momentum of the free state when the final bound state is coupled to the continuum electron, and O^L is the multiple operator inducing the transition.

As in the calculation of bound–bound radiative transitions, (65) may be decomposed into an angular part and a radial part,

$$S = \sum_{\kappa J_{\rm T}} \left| \sum_{\alpha\beta} < \psi_{\rm f}, \kappa; J_{\rm T} || Z^L_M(\alpha, \beta) || \psi_{\rm i} > \right.$$
$$\left. < \alpha || C^L || \beta > M^L_{\alpha\beta} \right|^2 \tag{66}$$

where $M^L_{\alpha\beta}$ is the one-electron radial integral for the multipole operator.

Since the continuum orbital is absent in the initial bound state, the creation operator $a^\dagger_{\tilde{\alpha}}$ must be chosen to be that of the free electron. Using the decoupling formula of Racah, the reduced matrix elements of the angular operator can be written as,

$$< \psi_,\kappa; J_{\rm T} || Z^L_M(\kappa, \beta) || \psi_{\rm i} > = (-1)^{J_{\rm T} + J_{\rm i} - L} [J_{\rm T}]^{1/2}$$
$$< \psi_{\rm f} || \tilde{a}_{\tilde{\beta}} || \psi_{\rm i} > \begin{Bmatrix} J_{\rm f} & j & J_{\rm T} \\ L & J_{\rm i} & j_\beta \end{Bmatrix} \tag{67}$$

where $J_{\rm i}$ and $J_{\rm f}$ are the total angular momenta of the initial and final states, j is the angular momentum of the free electron, and $\begin{Bmatrix} j_1 & j_2 & j_3 \\ j_4 & j_5 & j_6 \end{Bmatrix}$ is the Wigner $6j$ symbol. Substituting this into (66) results in,

$$S = \sum_{\kappa\beta\beta'} \sum_{J_{\rm T}} [J_{\rm T}] \begin{Bmatrix} J_{\rm f} & j & J_{\rm T} \\ L & J_{\rm i} & j_\beta \end{Bmatrix} \begin{Bmatrix} J_{\rm f} & j & J_{\rm T} \\ L & J_{\rm i} & j_{\beta'} \end{Bmatrix}$$
$$< \psi_{\rm f} || \tilde{a}_{\tilde{\beta}} || \psi_{\rm i} >< \psi_{\rm f} || \tilde{a}_{\tilde{\beta}'} || \psi_{\rm i} >< \kappa || C^L || \beta >$$
$$< \kappa || C^L || \beta' > M^L_{\kappa\beta} M^L_{\kappa\beta'} \tag{68}$$

The summation over $J_{\rm T}$ can be carried out analytically using the orthogonality relation of $6j$ symbols to give,

$$S = \sum_{\kappa\beta\beta'} \delta_{j_\beta j_{\beta'}} [j_\beta]^{-1} < \psi_{\rm f} || \tilde{a}_{\tilde{\beta}} || \psi_{\rm i} >< \psi_{\rm f} || \tilde{a}_{\tilde{\beta}'} || \psi_{\rm i} >$$
$$< \kappa || C^L || \beta >< \kappa || C^L || \beta' > M^L_{\kappa\beta} M^L_{\kappa\beta'} \tag{69}$$

Note that the condition $j_\beta = j_{\beta'}$ in the summation also implies $l_\beta = l_{\beta'}$, since only basis states with the same parity can mix in $\psi_{\rm i}$.

5.2. Multipole radial integrals

The radial integrals $M^L_{\kappa\beta}$ are the same as those involved in the the calculation of bound–bound radiative transitions, with a free electron replacing one of the bound orbitals. They may be calculated with the fully relativistic expressions of ref. 32. These expressions depend on both the photon and the ejected photo-electron energies. However, when the photon energy is not too high, the nonrelativistic limits of the multipole operators suffices. Using nonrelativistic multipole operators to evaluate radial integrals is the default of the program.

Unlike in bound–bound radiative transitions, the radial integrals now depend on the photo-electron energy. To reduce

computing time when cross sections at a large number of collision energy points are needed, the $M^L_{\kappa\beta}$ are calculated on an internal grid for the photo-electron energy. The integrals needed at other energies are interpolated using this grid. The grid points may be specified from the input, or if not specified it is generated according to the photo-electron energies where the cross sections are to be calculated. For highly charged ions, where no Cooper minimum is present, few points are needed for accurate interpolation. However, when the PI cross sections show Cooper minima in the low-energy region, which often occurs in neutral or near neutral ions, a dense grid should be used. On the other hand, the DW approximation at such low energies in neutral or near neutral ions is rather inaccurate [51].

6. Autoionization and dielectronic recombination

In the first-order perturbation theory, the autoionization (AI) rate can be written as,

$$A^a = 2\sum_\kappa \left| < \psi_\mathrm{f}, \kappa; J_\mathrm{T} M_\mathrm{T}| \sum_{i<j} \frac{1}{r_{ij}} |\psi_\mathrm{i} > \right|^2 \tag{70}$$

where ψ_i is the autoionizing state, ψ_f is the final state that has one less electron than ψ_i, κ is the relativistic angular quantum number of the free electron whose wave function is normalized as discussed in Sect. 3. The total angular momentum of the coupled final state must be equal to that of ψ_i, i.e., $J_\mathrm{T} = J_\mathrm{i}$ and $M_\mathrm{T} = M_\mathrm{i}$. After the separation of the angular and radial integrals we have,

$$A^a = 2[J_\mathrm{i}]^{-1} \sum_\kappa \Big| \sum_{k,\alpha\gamma\delta} < \psi_\mathrm{f}, \kappa; J_\mathrm{T}||Z^k(\alpha,\gamma) \cdot Z^k(\kappa,\delta)||\psi_\mathrm{i} > P^k(\kappa\delta;\alpha\gamma)\Big|^2 \tag{71}$$

where γ and δ are the doubly excited bound orbitals in ψ_i, α is the orbital that makes the internal transition in ψ_f, and P^k is the radial integral as defined in the expression for the DW collision strength of electron impact excitation, except that one of the free orbitals is replaced by a bound orbital. For autoionization of complex ions, the radial integrals P^k with the same set of bound orbitals, α, γ, and δ, often appear in many different transitions. However, the energies of the free electrons in these integrals are different due to the conservation of energy. It is computationally demanding to calculate such integrals for each transition individually. Fortunately, the dependence of P^k on the free electron energy is rather weak, as noticed by Oreg et al. [52]. Therefore, it is possible to calculate P^k at a few energies, and the integrals at actual transition energies are obtained by interpolation from these values. Usually for a given class of transitions, a three-point grid spanning the entire range of transition energies is sufficient.

The inverse process of AI is radiationless electron capture, sometimes called dielectronic capture (DC). The cross sections for DC are related to AI rates through the detailed balance. DC is a resonant process, which only occurs at certain energies. These resonances are extremely narrow, and in most applications it is more appropriate to characterize each resonance by its resonance strength, which is the cross section integrated over energy. In atomic units, the DC strength can be written as

$$S_\mathrm{DC} = \frac{g_\mathrm{i}}{2g_\mathrm{f}} \frac{\pi^2}{E_\mathrm{if}} A^a \tag{72}$$

where g_i and g_f are the statistical weights of the autoionizing state formed by DC and the target state before DC, respectively, and E_if is the resonance energy.

The autoionizing states formed by DC may either autoionize, or radiatively decay. Radiative decay to the states below the ionization limit completes the dielectronic recombination process, or DR. Sometimes, the final state of decay lies above the ionization limit and may further decay to yield DR or autoionize. Therefore, the radiative branching ratio for DR can be expressed as,

$$B(i) = \frac{\sum_k A^r(i\to k) + \sum_a A^r(i\to a)B(a)}{\sum_{k'} A^a(i\to k') + \sum_k A^r(i\to k) + \sum_a A^r(i\to a)} \tag{73}$$

where A^r represents radiative decay rates, k denotes levels below the ionization limit, a denotes levels that may further autoionize, and k' are the final levels of autoionization. In most cases, the effect of radiative decay to autoionizing levels is small, and an approximate expression for the branching ratio may be used by dropping the final term in both the numerator and denominator of (73), that is,

$$B(i) = \frac{\sum_k A^r(i\to k)}{\sum_{k'} A^a(i\to k') + \sum_k A^r(i\to k)} \tag{74}$$

This approximation turns out to be fairly good even if the decay to autoionizing levels is not completely negligible as demonstrated and explained in refs. 53 and 54. The DR strength S_DR is the product of DC strength and the branching ratio.

In plasma modeling, the DR rate coefficients, α_DR, for electrons in the Maxwellian distribution is often needed, which can be expressed as,

$$\alpha_\mathrm{DR}(T) = \frac{h^3}{(2\pi m_\mathrm{e} k_\mathrm{B} T)^{3/2}} \sum_i \frac{g_\mathrm{i}}{2g_\mathrm{f}} A^a(i\to f) B(i) \exp\left(-\frac{E_\mathrm{if}}{k_\mathrm{B}T}\right) \tag{75}$$

where T is the electron temperature, m_e is the electron mass, h is the Planck constant, and k_B is the Boltzmann constant. Since rate coefficients are not fundamental atomic parameters, atomic units are not used in this expression.

7. Sample applications

FAC has been used in a wide range of applications since its public release. Brief mention of its application in astronomy, magnetic fusion, and laser-produced plasma has been made already in Sect. 1. To further illustrate the reliability of FAC, we

Table 1. Comparison of energy levels (relative to the ground state) for the $n = 2$ states of N-like iron. The HULLAC, MCDF, and Breit–Pauli R-matrix (BPRM) results are from ref. 55.

		Energy (eV)				
Index	Level	Experiment	Present	HULLAC	MCDF	BPRM
0	$2s^2 2p^3\ ^4S^o_{3/2}$	0	0	0	0	0
1	$2s^2 2p^3\ ^2D^o_{3/2}$	17.1867	17.386	17.3514	17.4848	17.400
2	$2s^2 2p^3\ ^4D^o_{5/2}$	21.8373	22.657	22.4259	22.2628	21.376
3	$2s^2 2p^3\ ^2P^o_{1/2}$	32.2694	32.205	31.9788	32.1682	32.245
4	$2s^2 2p^3\ ^4S^o_{3/2}$	40.0890	40.501	40.0720	40.0987	39.908
5	$2s2p^4\ ^4P_{5/2}$	93.3266	93.939	93.4074	93.2280	93.198
6	$2s2p^4\ ^4P_{3/2}$	101.769	102.328	101.5300	101.906	101.30
7	$2s2p^4\ ^4P_{1/2}$	104.486	105.079	104.3240	104.592	103.99
8	$2s2p^4\ ^2D_{3/2}$	129.262	131.252	130.5768	129.635	129.91
9	$2s2p^4\ ^2D_{5/2}$	131.220	133.391	132.5973	131.506	131.65
10	$2s2p^4\ ^2S_{1/2}$	148.193	149.951	149.3152	148.891	148.595
11	$2s2p^4\ ^2P_{3/2}$	154.042	156.689	156.2177	155.532	154.967
12	$2s2p^4\ ^2P_{1/2}$	166.144	168.767	167.9513	167.437	154.967
13	$2p^5\ ^2P_{3/2}$	242.330	246.221	245.6736	244.0624	243.455
14	$2p^5\ ^2P_{1/2}$	255.680	259.855	258.9285	257.3803	256.768

provide in the following some simple calculations and compare the results with previous work. As an example of FAC's utility for energy level and oscillator strength calculations, we show in Tables 1 and 2 the energies and dipole oscillator strengths of $n = 2$ states of N-like iron. The results calculated with FAC agrees well with previous calculations using different theoretical approaches and experimental values.

Figure 1 shows the comparison of EIE collision strengths from the ground state to the $n = 2$ states of Be-like iron calculated with FAC and those of ref. 57. Because the EIE calculation in FAC is based on the DW approximation, resonace exciatation must be included with the independent process isolated resonance method. For highly charged ions, this method has been shown to be comparable in accuracy to the more sophisticated scattering calculations using the R-matrix method [58]. However, as channel coupling becomes more important in near neutral ions at low incident energies, the DW results may become increasingly unreliable, as indicated in ref. 59.

The ionization cross sections of $2s$ and $2p$ electrons for the ground state of Ne-like iron are calculated with FAC in CBE, relativistic DW, and BED approximations. The results are shown in Fig. 2. The relativistic DW cross sections of ref. 46 and those recommended in ref. 60 in their ionization equilibrium calculation for iron, which are based on the nonrelativistic DW results of ref. 61, are also presented for comparison. It is seen that the present CBE cross sections agrees with those of ref. 61 very well. The present DW results are slightly smaller than those of ref. 46, though the differences are within 10%. The BED cross sections are significantly smaller at low energies, which is due to the scaling factor discussed above.

Figure 3 shows the photoionization cross sections calculated with FAC and the comparison with those of ref. 51. Only electric dipole operators are included in the calculations. The photoelectron energy grid used in the FAC calculation is lightly different from that used in ref. 51. Our results shown in Table 3 are the interpolated values at their energy grid. The ioniza-

Table 2. Comparison of dipole oscillator strengths ($\geq$0.0001) for $2s^2 2p^3 - 2s2p^4$ transitions of N-like iron. The BPRM results are from ref. 56.

Lower	Upper	Present	NIST	BPRM
0	5	0.0494	0.0520	0.0503
0	6	0.0390	0.0413	0.0392
0	7	0.0209	0.0221	0.0208
0	8	0.0024	0.0026	0.0021
0	10	0.0010	0.0010	0.0009
0	11	0.0043	0.0045	0.0040
1	5	0.0035	0.0038	0.0033
1	6	0.0003	0.0004	0.0003
1	7	0.0004	0.0005	0.0004
1	8	0.0739	0.0780	0.0742
1	10	0.0290	0.0300	0.0289
1	11	0.0174	0.0181	0.0187
1	12	0.0146	0.0151	0.0148
2	5	0.0011	0.0012	0.0011
2	6	0.0001	0.0001	0.0001
2	9	0.0593	0.0630	0.0599
2	11	0.0856	0.0890	0.0868
3	7	0.0010	0.0011	0.0010
3	8	0.0136	0.0146	0.0141
3	10	0.0612	0.0640	0.0622
3	11	0.0270	0.0284	0.0272
3	12	0.0053	0.0057	0.0057
4	5	0.0003	0.0003	0.0003
4	6	0.0010	0.0011	0.0010
4	8	0.0017	0.0020	0.0018
4	9	0.0234	0.0250	0.0242
4	10	0.0025	0.0030	0.0026
4	11	0.0165	0.0167	0.0169
4	12	0.0671	0.0700	0.0679

Table 3. Comparison of ionization energies (eV) and PI cross sections (Mb) of $1s^22s \rightarrow 1s^2$, $1s^22p_{1/2} \rightarrow 1s^2$, and $1s^22p_{3/2} \rightarrow 1s^2$ for Li-like iron. The energy grid is indicated by the photon energy in threshold units. The first entries are the present results interpolated to the energy grid used in ref. 51, and the second entries are the results in ref. 51.

		E_{ph}/E_{th}					
Shell	E_{th}	1.01	1.20	2.00	3.00	4.00	6.00
$2s_{1/2}$	2046.5	2.35×10^{-2}	1.65×10^{-2}	5.47×10^{-3}	2.13×10^{-3}	1.05×10^{-3}	3.67×10^{-4}
	N/A	2.28×10^{-2}	1.62×10^{-2}	5.44×10^{-3}	2.13×10^{-3}	1.06×10^{-3}	3.74×10^{-4}
$2p_{1/2}$	1997.6	2.37×10^{-2}	1.42×10^{-2}	2.89×10^{-3}	7.74×10^{-4}	2.93×10^{-4}	7.12×10^{-5}
	2000.5	2.24×10^{-2}	1.36×10^{-2}	2.84×10^{-3}	7.65×10^{-4}	2.91×10^{-4}	7.06×10^{-5}
$2p_{3/2}$	1981.1	2.36×10^{-2}	1.40×10^{-2}	2.84×10^{-3}	7.54×10^{-4}	$2.8 \times 10^{E-4}$	6.82×10^{-5}
	1984.5	2.23×10^{-2}	1.35×10^{-2}	2.79×10^{-3}	7.43×10^{-4}	2.81×10^{-4}	6.77×10^{-6}

Fig. 1. Comparison of collision strengths of excitation from the ground state to $n = 2$ states of Be-like iron. Filled circles are the present results. Continuous lines are those of ref. 57. The numbers on the lines are the upper level indexes in the energy order counting from 0.

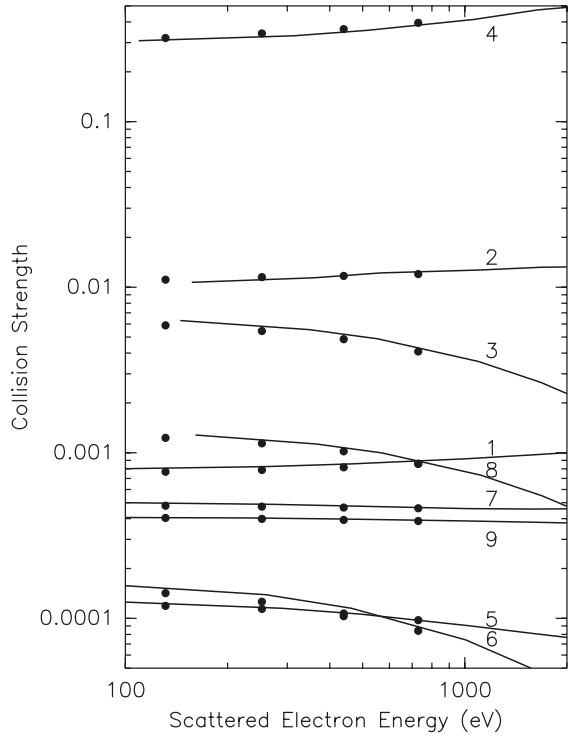

tion potentials and PI cross sections for the $1s^22s \rightarrow 1s^2$, $1s^22p_{1/2} \rightarrow 1s^2$, and $1s^22p_{3/2} \rightarrow 1s^2$ transitions are listed. The agreement is generally good to within a few percent.

Savin et al. [62] measured the $\Delta n = 0$ DR cross sections of O-like and F-like iron using the heavy-ion test storage ring and compared the experimental results with various theoretical calculations, all of them in the DW approximation. The multiconfiguration Dirac–Fork (MCDF) and Breit–Pauli (MCBP) calculations presented in their paper are shown to agree with the measurement to within 20%–30%. Recently, Pradhan et al. [63] calculated the $\Delta n = 0$ DR of F-like iron using the CC approximation and found those results to agree with experiment to within a similar percentage.

Fig. 2. Cross sections for the direct ionization of $2s$ and $2p$ subshells of Ne-like iron. The relativistic cross sections for $3p_{1/2}$ and $3p_{3/2}$ subshells are summed together.

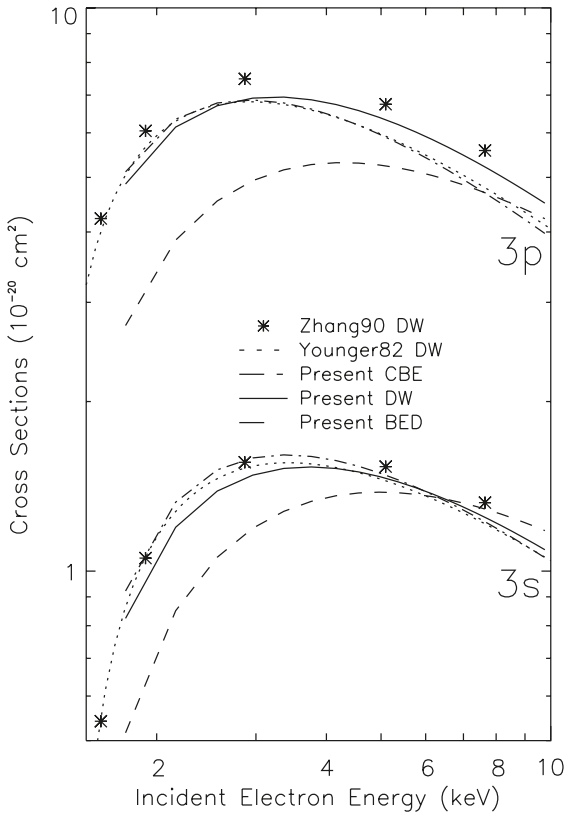

We have also calculated DR resonance strengths and rate coefficients of F-like iron for comparison with the experimental and previous theoretical results. The target states of the F-like iron include the configuration mixing within the $n = 2$ complexes. There are only two excitation channels for the $\Delta n = 0$ DR, corresponding to the core transitions $2s^22p^5P_{3/2} \rightarrow 2s^22p^5P_{1/2}$ and $2s^22p^5P_{3/2} \rightarrow 2s2p^6S_{1/2}$, which have measured transition energies of 12.7182 and 132.0063 eV, respectively. The theoretical resonance energies are adjusted according to these experimental transition energies. The doubly excited states of the Ne-like iron include the configuration mixing within the same $nln'l'$ complex.

Fig. 3. Comparison of the energy-weighted resonance strengths of F-like iron. The top panel is for $P_{3/2} \rightarrow P_{1/2}$ channel and the bottom panel is for $P_{3/2} \rightarrow S_{1/2}$ channel. The filled diamonds are the present results, open diamonds and filled circles are the MCDF calculations and experimental results of Savin et al. [62]. Note that the weighting factors of the resonance strengths plotted in Figs. 6 and 7 of ref. 62 are that of the highest energy resonances in each complex. The data plotted here include a small corrections factor (∼10%) for the first three points in both panels.

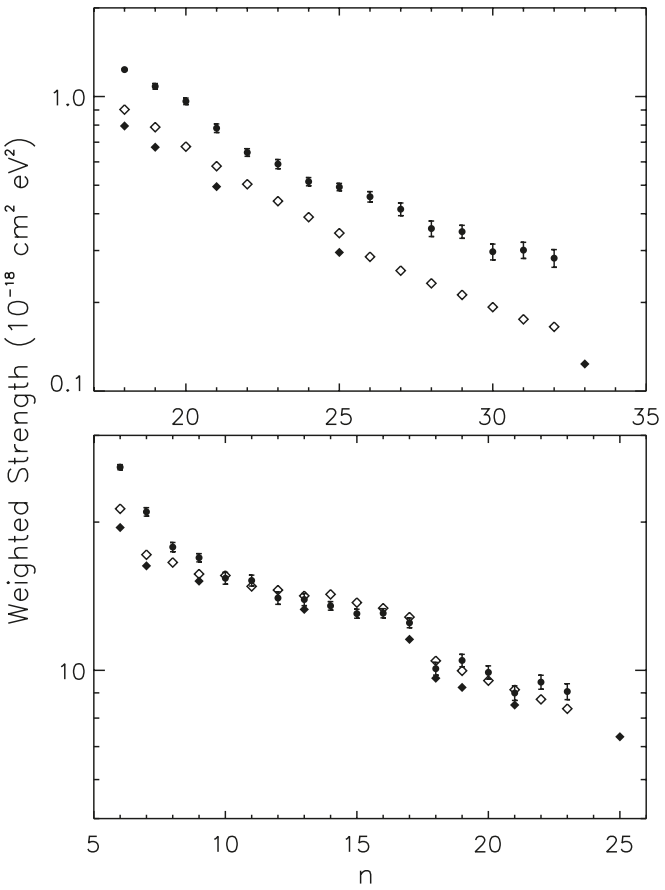

The $P_{3/2} \rightarrow P_{1/2}$ channel starts to open at $n' = 6$ for the spectator electron, and the $P_{3/2} \rightarrow S_{1/2}$ channel starts to open at $n' = 18$. The orbital angular momentum l' of up to 12 are included. Detailed calculations are carried out for $n' = 6$, 7, 9, 13, 17, 18, 19, 21, 25, 33, 49, and 60. DR rate coefficients for other values of $n' < 60$ are obtained by interpolation and for $n' > 60$ by extrapolation using the n'^{-3} scaling relation.

In Fig. 3, we show the energy-weighted resonance strengths as a function of n'. The strength for an entire n' complex is calculated as

$$S_n = \sum_i E_{\rm if} S_{\rm DC} B(i) \tag{76}$$

which removes the trivial dependence on the resonance energies. The approximate branching ratio given by (74) is used. Along with the present results, the MCDF calculations and the experimental results of ref. 62 are also shown. The present results seem to be systematically lower than the MCDF calculations by ∼10%–15%, and both theoretical results are smaller

Fig. 4. Comparison of the $\Delta n = 0$ DR rate coefficients of F-like iron. The dotted line is the present result for $P_{3/2} \rightarrow P_{1/2}$ channel, the broken line is the present result for $P_{3/2} \rightarrow S_{1/2}$ channel, the continuos line is the present total rate coefficients, the dash-dot, and the long-dash lines are the MCDF calculations and experimental results of ref. 62.

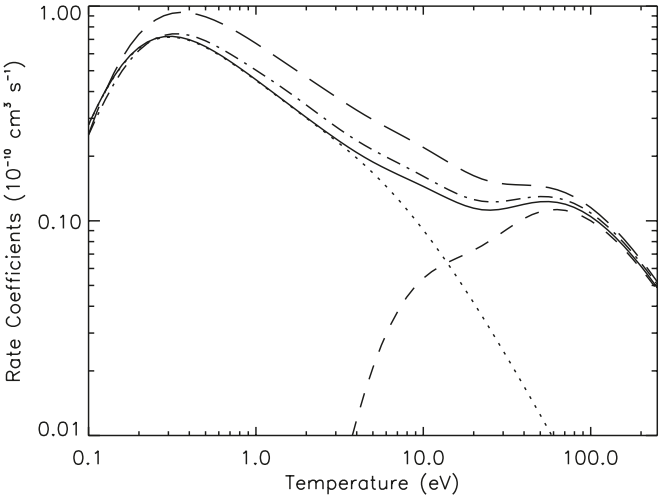

than the measurements. Figure 4 shows the comparison of total $\Delta n = 0$ DR rate coefficients as a function of temperature. At temperatures above 100 eV, the present calculations agree with the experimental results and the MCDF results to within a few percent. At lower temperatures, the difference between the present calculations and the MCDF results is less than 15%, and the difference between the present calculations and the measurements is ∼10%–40%.

8. Conclusions

In conclusion, we have described an integrated software package, the flexible atomic code (FAC), for the computation of various atomic radiative and collisional processes. The program is fully relativistic and implements efficient methods for distorted wave approximation, which is most useful for modeling spectral properties of highly charged ions.

Acknowledgements

The author would like to thank Peter Beiersdorfer for extensive comments on the manuscript. The initial development of FAC was supported by NASA through Chandra Postdoctoral Fellowship Award Number PF01-10014 issued by the Chandra X-ray Observatory Center, which is operated by Smithsonian Astrophysical Observatory for and on behalf of NASA under contract NAS8-39073. Work at Lawrence Livermore National Laboratory was performed under the auspices of the US Department of energy under contract W-7405-ENG-48.

References

1. M.F. Gu. Astrophys. J. **582**, 1241 (2003).
2. M.F. Gu. Astrophys. J. **589**, 1085 (2003).
3. M.F. Gu. Astrophys. J. **590**, 1131 (2003).

4. M.F. Gu. Astrophys. J. **593**, 1249 (2003).
5. M. Bitter, M.F. Gu, L.A. Vainshtein, P. Beiersdorfer, T. Bertschinger, O. Marchuk, R. Bell, B. Leblanc, K.W. Hill, D. Johnson, and L. Roquemore. Phys. Rev. Lett. **91**, 265001 (2003).
6. H. Chen, M.F. Gu, P. Beiersdorfer, K.R. Boyce, G.V. Brown, S.M. Kahn, R.L. Kelley, C.A. Kilbourne, F.S. Porter, and J.H. Scofield. Astrophys. J. **646**, 653 (2006).
7. H. Chen, M.F. Gu, E. Behar, G.V. Brown, S.M. Kahn, and P. Beiersdorfer. Astrophys. J. Suppl. **168**, 319 (2007).
8. M.F. Gu, P. Beiersdorfer, G.V. Brown, H. Chen, D.B. Thorn, and S.M. Kahn. Astrophys. J. **657**, 1172 (2007).
9. S.B. Hansen. Phys. Rev. E, **71**, 016408 (2005).
10. J.Y. Zhong, C. Wang, J. Zhang, X. Lu, G. Zhao, J.L. Zeng, M.F. Gu, and S.J. Wang. Phys. Rev. A, **70**, 053803 (2004).
11. D.L. Robbins, A.Y. Faenov, T.A. Pikuz, H. Chen, P. Beiersdorfer, M.J. May, J. Dunn, K.J. Reed, and A.J. Smith. Phys. Rev. A, **70**, 022715 (2004).
12. H. Chen, P. Beiersdorfer, M.F. Gu, L.A. Heeter, J. Lepson, D.A. Liedahl, K.L. Naranjo-Rivera, and E. Träbert. Astrophys. J. **611**, 598 (2004).
13. G. Liang, G. Zhao, and J.R. Shi. Mon. Not. R. Astron. Soc. **368**, 196 (2006).
14. E. Landi and M.F. Gu. Astrophys. J. **640**, 1171 (2006).
15. A. Hibbert. Comput. Phys. Commun. **9**, 141 (1975).
16. W. Eissner, M. Jones, and H. Nussbaumer. Comput. Phys. Commun. **8**, 270 (1974).
17. R.D. Cowan. Theory of atomic structure and spectra. University of California Press, Berkeley. 1981.
18. C. Froese Fischer, T. Brage, and P. Jonsson. Computational atomic physics: An MCHF approach. Institute of Physics Publishing, Bristol, UK. 2000.
19. I.P. Grant, B.J. Mckenzie, P.H. Norrington, D.F. Mayers, and N.C. Pyper. Comput. Phys. Commun. **21**, 207 (1980).
20. M.Y. Amusia and L.V. Chernysheva. Computation of atomic processes: A handbook for ATOM programs. Institute of Physics Publishing, Bristol, UK. 1997.
21. A. Bar-Shalom, M. Klapisch, and J. Oreg. J. Quant. Spectrosc. Radiat. Transfer, **71**, 169 (2001).
22. D.H. Sampson, H.L. Zhang, A.K. Mohanty, and R.E.H. Clark. Phys. Rev. A, **40**, 604 (1989).
23. H.L. Zhang, D.H. Sampson, and A.K. Mohanty. Phys. Rev. A, **40**, 616 (1989).
24. M. Klapisch, J.L. Schwob, B.S. Fraenkel, and J. Oreg. J. Opt. Soc. Am. **67**, 148 (1977).
25. L.V. Chernysheva and V.L. Yakhontov. Comput. Phys. Commun. **119**, 232 (1999).
26. I.G. Young and P.H. Norrington. Comput. Phys. Commun. **83**, 215 (1994).
27. I.P. Grant. Comput. Phys. Commun. **11**, 397 (1976).
28. G. Gaigalas, Z. Rudzikas, and C.F. Fischer. J. Phys. B, **30**, 3747 (1997).
29. G. Gaigalas, S. Fritzsche, and I.P. Grant. Comput. Phys. Commun. **139**, 263 (2001).
30. B.R. Judd. Second quantization in atomic spectroscopy. Johns Hopkins Press, Baltimore, Md. 1967.
31. A. Bar-Shalom, M. Klapisch, and J. Oreg. Phys. Rev. A, **38**, 1773 (1988).
32. I.P. Grant. J. Phys. B, **7**, 1458 (1974).
33. M.J. Seaton. Adv. Atom. Mol. Phys. **11**, 83 (1975).
34. K.A. Berrington, W.B. Eissner, and P.H. Norrington. Comput. Phys. Commun. **92**, 290 (1995).
35. W.B. Eissner and M.J. Seaton. J. Phys. B, **5**, 2187 (1972).
36. W.B. Eissner. Comput. Phys. Commun. **114**, 295 (1998).
37. P.L. Hagelstein and R.K. Jung. Atom. Data Nucl. Data Tables, **37**, 121 (1987).
38. G. Chen. Phys. Rev. A, **53**, 3227 (1996).
39. E. Haug. Solar Phys. **25**, 425 (1972).
40. E. Haug. Solar Phys. **71**, 77 (1981).
41. T. Fujimoto, H. Sahara, T. Kawachi, T. Kallstenius, M. Goto, H. Kawase, T. Furukubo, T. Maekawa, and Y. Yerumichi. Phys. Rev. E, **54**, 2240 (1996).
42. P. Beiersdorfer, D.A. Vogel, K.J. Reed, V. Decaux, J.H. Scolfield, K. Widmann, G. Hözer, E. Föster, O. Wehrhan, D.W. Savin, and L. Schweikhard. Phys. Rev. A, **53**, 3974 (1996).
43. E. Takács, E.S. Meyer, J.D. Gillaspy, J.R. Roberts, C.T. Chander, L.T. Hudson, R.D. Deslattes, C.M. Brown, J.M. Laming, J. Dubau, and M.K. Inal. Phys. Rev. A, **54**, 1342 (1996).
44. M.K. Inal and J. Dubau. J. Phys. B, **20**, 4221 (1987).
45. H.L. Zhang, D.H. Sampson, and R.E.H. Clark. Phys. Rev. A, **41**, 198 (1990).
46. H.L. Zhang and D.H. Sampson. Phys. Rev. A, **42**, 5378 (1990).
47. L.B. Golden and D.H. Sampson. J. Phys. B, **10**, 2229 (1977).
48. L.B. Golden and D.H. Sampson. J. Phys. B, **13**, 2645 (1980).
49. C. Fontes, D.H. Sampson, and H.L. Zhang. Phys. Rev. A, **48**, 1975 (1993).
50. Y. Kim and M.E. Rudd. Phys. Rev. A, **50**, 3954 (1994).
51. H.L. Zhang. Phys. Rev. A, **57**, 2640 (1998).
52. J. Oreg, W.H. Goldstein, M. Klapisch, and A. Bar-Shalom. Phys. Rev. A, **44**, 1750 (1991).
53. E. Behar, P. Mandelbaum, J.L. Schwob, A. Bar-Shalom, J. Oreg, and W.H. Goldstein. Phys. Rev. A, **52**, 3770 (1995).
54. E. Behar, P. Mandelbaum, J.L. Schwob, A. Bar-Shalom, J. Oreg, and W.H. Goldstein. Phys. Rev. A, **54**, 3070 (1996).
55. D.W. Savin, E. Behar, S.M. Kahn, J. Linkemann, G. Gwinner, A.A. Saghiri, M. Schmitt, M. Grieser, R. Repnow, D. Schwalm, A. Wolf, T. Bartsch, A. Müller, S. Schippers, N.R. Badnell, M.H. Chen, and T.W. Gorczyca. Ap. J. Suppl. **138**, 337 (2002).
56. H.L. Zhang and A.K. Pradhan. Mon. Not. R. Astron. Soc. **313**, 13 (2000).
57. G. Chen and P.P. Ong. Phys. Rev. A, **58**, 1183 (1998).
58. M.F. Gu. Phys. Rev. A, **70**(6), 062704 (2004).
59. D.H. Madison, A. Dasgupta, K. Bartschat, and D. Vaid. J. Phys. B, **37**, 1073 (2004).
60. M. Arnaud and J. Raymond. Astrophys. J. **398**, 394 (1992).
61. S.M. Younger. J. Quant. Spectrosc. Radiat. Transfer, **27**, 541 (1982).
62. D.W. Savin, S.M. Kahn, J. Linkemann, A.A. Saghiri, M. Schmitt, M. Grieser, R. Repnow, D. Schwalm, A. Wolf, T. Bartsch, C. Brandau, A. Hoffknecht, A. Müller, S. Schippers, M.H. Chen, and N.R. Badnell. Astrophys. J. Suppl. **123**, 687 (1999).
63. A.K. Pradhan, S.N. Nahar, and H.L. Zhang. Astrophys. J. **549**, L265 (2001).